Electrochemical Production of Hydroxyl Radical at Polycrystalline Nb-Doped TiO_2 Electrodes and Estimation of the Partitioning between Hydroxyl Radical and Direct Hole Oxidation Pathways

Janet M. Kesselman, Oleh Weres, Nathan S. Lewis, and Michael R. Hoffmann*

W. M. Keck Laboratories, California Institute of Technology, Pasadena, California 91125

Received: August 30, 1996; In Final Form: October 29, 1996[⊗]

The use of TiO_2 as a photocatalyst for the destruction of organic chemical pollutants in aqueous systems has been extensively studied. One obstacle to the effective utilization of these systems is the relatively inefficient use of the solar spectrum by the photocatalyst. In addition, light delivery to the photocatalyst can be impeded by UV-absorbing components in mixed effluent streams. We present a novel use of TiO_2 as a catalyst for the oxidative degradation of organic compounds in water that uses a potential source instead of light to generate reactive oxidants. Application of an anodic bias of $>+2$ V vs NHE to titanium electrodes coated with niobium-doped, polycrystalline TiO_2 particles electrochemically generates hydroxyl radicals at the TiO_2 surface. This process has been demonstrated to efficiently degrade a variety of environmentally important pollutants. In addition, these electrodes offer a unique opportunity to probe mechanistic questions in TiO_2 catalysis. By comparing substrate degradation rates with increases in current density upon substrate addition, the extent of degradation due to direct oxidation and •OH oxidation can be quantified. The branching ratio for these two pathways depends on the nature of the organic substrate. Formate is shown to degrade primarily via a hydroxyl radical mechanism at these electrodes, whereas the current increase data for compounds such as 4-chlorocatechol indicate that a higher percentage of their degradation may occur through direct oxidation. In addition, the direct oxidation pathway is shown to be more important for 4-chlorocatechol, a strongly adsorbing substrate, than for 4-chlorophenol, which does not adsorb strongly to TiO_2.

Introduction

The use of TiO_2 as a photocatalyst for the destruction of organic pollutants in aqueous waste streams has been studied extensively.[1,2] Light absorption in TiO_2 at $\lambda \leq 385$ nm effects the promotion of an electron from the valence band to the conduction band of the semiconductor.[2] This excitation process creates an electronic charge carrier in the conduction band and an electron vacancy (a hole) in the valence band. Because the valence band edge of TiO_2 occurs at approximately $+3.2$ V vs the normal hydrogen electrode, NHE, at pH 0 (the position of the band edge is pH dependent[3,4]), the hole is a very powerful oxidizing agent and is capable of oxidizing a variety of organic molecules as well as generating hydroxyl radicals in water. Illuminated slurries of TiO_2 have been shown to oxidize a wide range of organic pollutants, leading to the formation of CO_2.[5−8] There is a great deal of interest in using TiO_2 for waste treatment due to the low cost of the TiO_2 catalyst as well as the potential for using sunlight as the energy source. However, the quantum yields for photodegradation of organics in aqueous solution are low.[9,10] Commercial applications employ systems involving immobilization of the photocatalyst onto a solid support and the use of UV lamps instead of sunlight to enable continuous operation of the reactor.[11]

In a novel application of TiO_2 as a catalyst for the destruction of organic pollutants, new polycrystalline TiO_2 electrodes, that are capable of generating hydroxyl radicals under an anodic bias (Figure 1)[12−14] have been developed.

$$H_2O \rightarrow HO^{\bullet} + H^+ + e^- \qquad E_0 = -2.74\ \text{V} \qquad (1)$$

Kamat and co-workers have used an applied bias to enhance the separation of photogenerated charge carriers in polycrystalline TiO_2 electrodes.[15,16] However, our electrode system[12−14] is the first, to our knowledge, to generate hydroxyl radicals at the surface of TiO_2 using only an applied voltage. Significant levels of hydroxyl radical generation are not observed at typical metal electrodes, such as platinum, because the four-electron oxidation of water to dioxygen occurs at a potential ($+1.23$ V at pH $= 0$) well below that required for the one-electron oxidation of water to •OH ($+2.74$ V at pH $= 0$).[17] Thus, most metal electrodes are sufficiently catalytic for the four-electron process that the O_2 production pathway predominates at potentials high enough to generate •OH. In contrast, these degenerately doped TiO_2 electrodes have been demonstrated to effectively destroy a variety of environmentally important pollutants in aqueous solutions.[12−14]

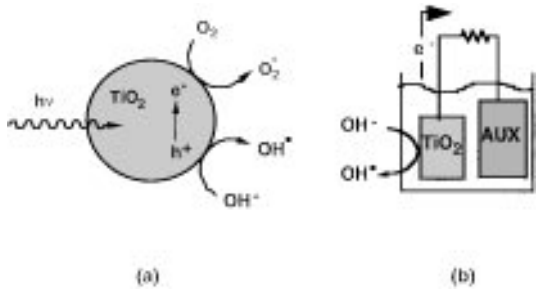

Figure 1. TiO_2 photocatalysis vs TiO_2 electrocatalysis: (a) schematic representation of the processes occurring in TiO_2 photocatalysis; (b) schematic representation of TiO_2 electrocatalysis.

The use of TiO_2 electrodes also allows the experimental determination of certain quantities that are not readily measurable on TiO_2 particles. In a previous study, we used single-crystal TiO_2 (rutile) electrodes to examine the possibility that oxygen reduction was rate limiting in the TiO_2-photocatalyzed decomposition of organic compounds in water.[18] Our primary

* To whom correspondence should be addressed.

[⊗] Abstract published in *Advance ACS Abstracts,* March 1, 1997.

S1089-5647(96)02669-7 CCC: $14.00

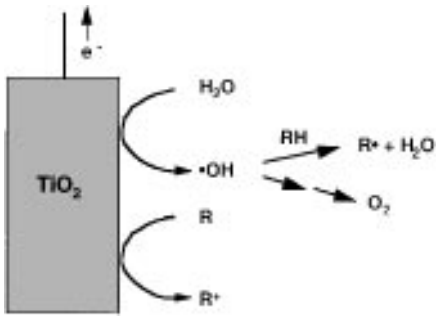

Figure 2. Schematic diagram illustrating differences in the expected current response between direct oxidation and hydroxyl radical-mediated oxidation pathways.

objective for this study was to investigate the production of hydroxyl radicals at the Nb-doped polycrystalline TiO_2 electrodes.

A major uncertainty in the field TiO_2 photocatalysis is whether oxidation occurs either by direct hole transfer or by hydroxyl radical attack; evidence in support of both mechanisms has been obtained.[19−25] Ideally, a direct measure of the amount of hydroxyl radical production, for example through use of radical traps, would be desirable.[26,27] However, common hydroxyl radical traps can be directly oxidized at very positive potentials, so alternative approaches were sought to distinguish between hydroxyl radical production and direct oxidation of the organic molecules.

Several different types of experiments were carried out in order to assess the production of hydroxyl radicals at degenerately doped, polycrystalline TiO_2 electrodes. The first protocol involved comparison of the degradation rates of a series of chlorinated acetates on TiO_2 to the known rate constants for the homogeneous reaction of these same reagents with hydroxyl radicals. The rate constants for homogeneous reactions of these acetates with hydroxyl radical follow the trend[25]

$$ClCH_2CO_2^- > Cl_2CHCO_2^- > CH_3CO_2^- \gg Cl_3CO_2^- \quad (2)$$

This trend occurs because the electronegative chlorine weakens the C-H bond, so the hydrogen atom in chloroacetate and dichloroacetate is more readily abstracted by the •OH relative to the hydrogen atom abstraction from acetate. Trichloroacetate, however, possesses no abstractable hydrogens and is degraded only slowly by hydroxyl radicals.

In contrast, the oxidation potentials of these acetates are expected to increase with an increasing degree of chlorination. Direct oxidation through hole transfer from the TiO_2 to the organic would thus be expected to follow the trend

$$CH_3CO_2^- > ClCH_2CO_2^- > Cl_2CHCO_2^- > Cl_3CO_2^- \quad (3)$$

Measurement of the degradation rates of the substituted acetates on polycrystalline TiO_2 can then determine whether the oxidation process is consistent with a direct electron transfer pathway or homogeneous hydroxyl radical attack.

A second set of experiments was designed to quantify the extent of degradation occurring through •OH attack relative to direct oxidation. Figure 2 shows the current-branching behavior expected during electrocatalysis at degeneratively doped TiO_2 electrodes. The rates of direct oxidation and •OH-mediated oxidation should have different kinetic dependencies on the concentration of the organic substrate. For oxidation mediated by hydroxyl radicals, water is the species being oxidized at the electrode surface. Since the water concentration is constant, the observed current for this pathway should be independent of the concentration of organic substrate. In contrast, for oxidation occurring by direct electron transfer, the current should increase as the concentration of organic substrate increases. Assuming that the observed current increase corresponds to direct one-electron oxidation, the magnitude of the current increase divided by the total degradation rate yields the percentage of substrate degradation that proceeds through the direct oxidation pathway. The magnitude of the increase in current observed upon addition of substrate can only be used to place an upper limit on the percentage of substrate degradation that occurs through a direct oxidation mechanism.

A third set of experiments involved the measurement of degradation rates of a wider range of oxidizable substrates in a flate plate electrochemical cell and the comparison of the measured degradation rates to the known rates of the corresponding homogeneous reactions with hydroxyl radical in aqueous solution.

Experimental Section

Chemicals. Sodium acetate trihydrate (99+%), sodium chloroacetate (98%), potassium dichloroacetate (98%), and sodium trichloroacetate (97%) were purchased from Aldrich Chemicals (Milwaukee, WI). Sodium azide (99.99+%), *tert*-butyl methyl ether (99.8%), dichlorophenoxyacetic acid (98%), sodium diisopropylmethylphosphonate (95%), sodium formate (99+%), and 2,2′-thiodiethanol {2-hydroxyethyl sulfide} (99+%) were also purchased from Aldrich. Sodium mono- and dibasic phosphate and sodium formate (99%) were purchased from EM (Gibbstown, NJ). 4-chlorophenol was purchased from Aldrich (Milwaukee, WI). 4-Chlorocatechol was purchased from TCI America (Portland, OR) and was purified by recrystallization from hot heptane. Except for the 4-chlorocatechol, all chemicals were used as received. All solutions were prepared using Millipore Milli-Q^{UV} Plus 18 MΩ cm resistivity deionized water.

Nb-Doped Polycrystalline TiO_2 Electrodes. Preparation of the Nb-doped TiO_2 electrodes has been described in detail elsewhere.[12−14] In general, the electrodes are made by coating a titanium substrate with Nb-doped TiO_2 particles, followed by annealing the film under hydrogen. The electrodes are produced by baking a slurry coat of TiO_2 doped with Nb_2O_5 at 4 mol% Nb on the titanium metal substrate. The resulting "green" oxide coating is then reduced in the presence of H_2 to reduce the Nb(V) to Nb(IV). One set of electrodes used in this work were cylindrical rods with diameters of 6.35 mm and lengths of approximately 35 mm with reactive surface areas of 7.6 cm^2. After an initial "break in" period, the electrode behavior was stable through the course of many experiments when operated at the low current densities used in this work. However, when the electrodes were operated at higher current densities, their lifetimes were significantly shortened. Extended use of the electrodes generally resulted in a gradual decrease in the observed current for a given electrode potential, sometimes followed by an increase in current. Identically prepared electrodes often displayed different absolute current densities at a given potential (see Table 2); thus, kinetic trends were evaluated for the same electrode operated in a controlled series of experiments.

Electrochemical Cells and Instrumentation. Most chemical degradation and electrochemical experiments were carried out in a two-compartment Pyrex cell (Figure 3). The TiO_2 working electrode described above and the $Hg/Hg_2SO_4/K_2SO_4$(aq) reference electrode (+0.64 vs NHE) were separated from the counter electrode (made from carbon fibers) by a fine porosity glass frit. The volume of solution in the working compartment was 60 or 500 mL, as noted in the figure captions.

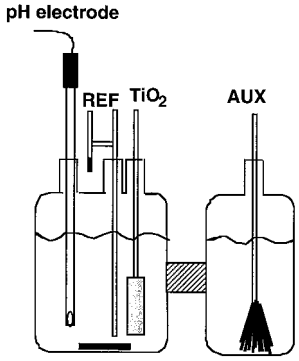

Figure 3. Schematic of the two-compartment cell used in this work. The TiO_2 working electrode and the $Hg/Hg_2SO_4/K_2SO_4$(satd) or standard calomel reference electrodes (SCE) were separated from the carbon fiber auxiliary electrode by a fine porosity glass frit.

In addition to the simple cell configuration depicted in Figure 3, a flat plate cell (FPC) reactor that incorporates a stack of closely spaced rectangular electrodes was used for kinetic measurements.[15] The plate electrodes ($12.7 \times 5.7 \times 0.05$ cm) are bipolar in that one face of the electrode operates as an anode, while the other face operates as a cathode. In the reactor cell, there are 30 stacked-plate electrodes with a total anode area of 0.18 m^2 operating a design current of 2.58 A at the voltage of 70 V. The volume of the core reactor is 0.75 L. Power is applied to the two electrodes at the ends of the stack only, and the polarity of voltage is periodically reversed. The Ti sheet employed is textured by cold rolling between patterned rollers (Rigidized Metals Corp., Buffalo, NY). The resulting uneven surface texture increases the amount of turbulence produced in water flowing past the bipolar electrodes, thereby improving mass transfer rates (i.e., turblent flow with Re = 2200). However, for the experiments described below the reactor was run in the batch mode.

An EG&G PAR Model 362 scanning potentiostat/galvanostat (Princeton, NJ) was used for experiments performed at constant current. Constant potential experiments were performed on a BAS Model CV50 Potentiostat (Lafayette, IN) using the bulk electolysis mode.

Analytical Methods. *(a) Ion Chromatography*. Acetate, azide, chloroacetate, dichloroacetate, 2,4-dichlorophenoxyacetate, trichloroacetate, and formate were analyzed by ion chromatography. Samples were withdrawn at given time intervals, and the substrate concentration was analyzed using a Dionex BioLC (Sunnyvale, CA) equipped with a pulsed electrochemical detector and an Omnipac PAX-500 analytical column. The eluants consisted of 1 mM NaOH(aq), 200 mM NaOH(aq), and 5% MeOH(aq) and were mixed in various ratios to achieve good separation between substrate and background electrolyte peaks with a minimum of analysis time. Since experiments were run in the presence of high concentrations of background electrolyte (either K_2SO_4 or phosphate), samples were diluted prior to analysis in order to avoid overloading the column.

(b) HPLC. 4-Chlorophenol, *p*-cresol, and 4-chlorocatechol were analyzed by high-pressure liquid chromatography (HPLC). A Hewlett-Packard ODS Hypersil, 5 μm, 100×2.1 mm column was used. The instrument was a Hewlett-Packard Series II 1090 liquid chromatograph. The eluants consisted of aqueous phosphoric acid (pH 3) and HPLC grade acetonitrile. To remove any particles that might clog the column, the samples were filtered with Gelman Acrodisc 4 CR PTFE 0.45 μm filters (Ann Arbor, MI) prior to analysis.

(c) CO_2 Production. CO_2 production was monitored by gas chromatography using a Carle AGC Series 400 gas chromatograph equipped with a Porapak QS column and a thermal conductivity detector (Loveland, CO). The oven temperature was maintained at 70 °C, and these conditions afforded good separation between air and CO_2 peaks. Standards were prepared from Na_2CO_3 dissolved in the same background electrolyte that was used in the degradation experiments. To initiate the analysis, 0.5 mL of the standard or sample was injected into a 2 mL glass vial with a Teflon septa cap. Prior to injection on the GC, 50 μm of concentrated H_2SO_4 was added to acidify the samples. A 15 μL aliquot of the head space was then injected onto the column. MBTE was determined by headspace GC (Tracor Model 540 with a OV-3 Megabore column) FID analysis, while the sulfur and phosphorus compounds were detected by FPD.

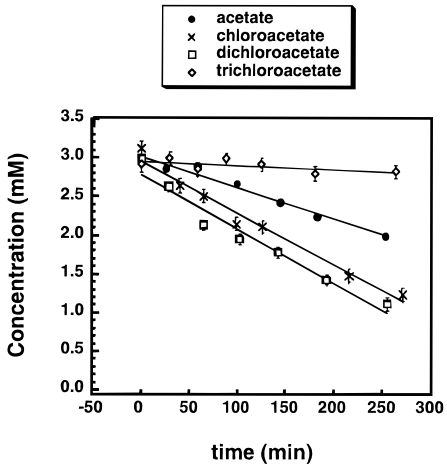

Figure 4. Concentration vs time data during the bulk electrolysis of substituted acetates at polycrystalline TiO_2 electrodes. Experimental conditions: 0.5 M phosphate buffer, pH = 6.4; 3 mM initial acetate concentration; current = 15 mA; 60 mL of solution in the working electrode compartment. Trichloroacetate shows almost no change in concentration during the 5 h experiment, consistent with its slow reaction rate with •OH. Chloroacetate and dichloroacetate react more quickly than acetate, as expected for an •OH abstraction process.

Results

Degradation of Chlorinated Acetates. Figure 4 depicts the time dependence of the concentrations of acetate, chloroacetate, dichloroacetate, and trichloroacetate during electrolysis at a TiO_2 electrode. These experiments were carried out in 0.5 M phosphate buffer (pH = 6.4), at a constant current of 15 mA. The trichloroacetate concentration was essentially constant over the course of the 5 h experiment, whereas significant decreases were observed in the chloroacetate and dichloroacetate concentrations over this same time period. Similar experiments were carried out using a pH stat to control the pH to 9.0 with potassium sulfate as the electrolyte. The results of these experiments are summarized in Table 1. For each set of experiments, the trend in reaction rate parallels the trend observed for the homogeneous reaction rate of •OH with the various acetates.

Current Density vs Solution Composition. As described in the Introduction, it is also informative to examine the dependence of the current density on the concentration of the organic substrate in the solution. Assuming that any increase in current density observed after addition of the organic species to the solution is due to the direct oxidation of this electroactive reagent, the magnitude of the current increase can be converted into an equivalent degradation rate of the organic substrate and compared to the observed degradation rate. If the number of electrons involved in the electrochemical reaction were known,

TABLE 1: Comparison between Reaction Rates of Acetate with •OH and TiO_2 Electrodes

I. substrate	II. k_{OH} (M^{-1} s^{-1})[a]	III. k_{meas} (min^{-1})[b]	IV. k_{meas} (min^{-1})[c]	V. k_{meas} (min^{-1})[d]
$CH_3CO_2^-$	(1-2) × 10^7	4.7×10^{-4}	1.6×10^{-4}	3.3×10^{-3}
		4.4×10^{-4}	2.6×10^{-4}	1.6×10^{-3}
			2.8×10^{-4}	
$ClCH_2CO_2^-$	(4-8) × 10^7	1.2×10^{-3}	1.0×10^{-3}	8.5×10^{-3}
		1.1×10^{-3}	5.6×10^{-4}	3.4×10^{-3}
		1.3×10^{-3}		
$Cl_2CHCO_2^-$	2.8×10^7	7.8×10^{-4}	3.5×10^{-4}	5.6×10^{-3}
		9.9×10^{-4}		3.8×10^{-3}
$Cl_3CO_2^-$	$<10^6$	$\sim 10^{-5}$	$\sim 10^{-5}$	$\sim 10^{-4}$

[a] Taken from ref 25. [b] 3 mM acetate, pH = 9.0, I = 15 mA, 0.1 M K_2SO_4, 500 mL cell. [c] 5 mM acetate, pH = 9.0, I = 10 mA, 0.1 M K_2SO_4, 500 mL cell. [d] 3 mM acetate, pH = 6.4, I = 15 mA, 0.5 M phosphate buffer, 60 mL cell.

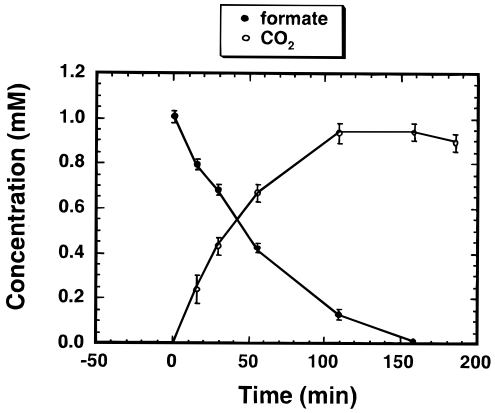

Figure 5. Concentration vs time data for the bulk electrolysis of formate at a polycrystalline TiO_2 electrode. Also shown are concentration vs time profiles for the appearance of CO_2 in the cell. The experimental conditions were as follows: I = 15 mA, 1 M phosphate buffer, pH = 6.4, 60 mL volume working compartment, closed cell.

this procedure would yield a quantitative measure of the kinetic branching ratio between the rate of direct oxidation and the rate of •OH production.

This experiment, in which the current density was monitored as a function of the concentration of the organic compound, was performed using formate, acetate, chloroacetate, trichloroacetate, 4-chlorophenol, or 4-chlorocatechol. Figure 5 shows the time dependence of the formate concentration, as well as the concurrent time dependence of the concentration of CO_2, which is formed stoichiometrically as a two-electron oxidation product of formate at the Nb-doped polycrystalline TiO_2 electrodes. The experiment was run in constant current mode with I = 15 mA (we note that this current is greater than the equivalent observed degradation rate for formate due to the competing pathway involving O_2 production), and the potential range observed during the experiment was 3.10 ± 0.01 V vs NHE. Figure 6a shows the current vs time data for an electrode held at 3.10 V vs NHE as formate is added. Additionally, Figure 6b depicts a plot of the magnitude of the observed current increase of the TiO_2 electrode as a function of the concentration of formate in the solution. A linear dependence of the current density on the formate concentration is expected for the direct oxidation of substrates that are dissolved homogeneously in the solution. For each of the compounds investigated, however, the magnitude of the current increase per unit change in substrate concentration decreased at higher total substrate concentrations. This behavior suggests that the direct oxidation pathway involves surface-sorbed species which saturate the available surface sites on the TiO_2 electrode at high substrate concentrations.

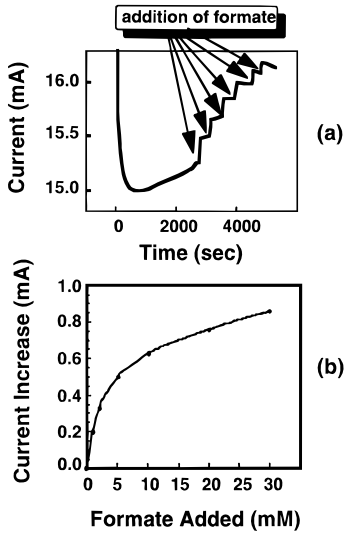

Figure 6. Current at a fixed potential of a polycrystalline Nb-doped TiO_2 electrode as a function of formate concentration. (a) Current vs time data for an electrode held at +3.1 V vs NHE in a 1 M phosphate solution at pH 6.4. As shown, the current increased abruptly when the formate was added to the solution. (b) Graph of the resulting current increase as a function of the total concentration of formate added to the solution. The graph displays a "saturation" behavior suggestive of electron transfer from adsorbed species.

TABLE 2: Degradation of Organics by a Direct Oxidation Pathway at TiO_2 Electrodes[a]

I. substrate	II. initial degradation rate (mM/min)	III. current increase (mA/mM)	IV. direct oxidation rate (calcd) (mM/min)	V. maximum % direct oxidation
formate	**0.0095**	**0.22**	**0.0011**[b]	**12**
4-chlorophenol	**0.0046**	**0.29**	**0.0030**	**65**
4-chloroatechol	**0.0047**	**0.44**	**0.0046**	**97**
acetate	**0.0023**	**0.14**	**0.0015**	**65**
	0.0065	0.10	0.0010	15
dichloroacetate	0.0089	<0.01	<0.001	<1
trichloroacetate	0.0002	<0.01	<0.001	<50

[a] Boldfaced type = electrode TiO_2-1, degradation at constant I = 15 mA. Plain type = electrode TiO_2-2, degradation at constant V = 2.9 V vs NHE. [b] Assuming two electrons transferred.

Table 2 shows the total degradation rates and maximum percent direct oxidation data for the different substrates. The initial degradation rates (determined from linear fits to the data obtained for the substrate concentration as a function of time) for the compounds studied are shown in the second column of Table 2. The following column shows the magnitude of the current increase upon addition of 1 mM substrate, while the fourth column shows the degradation rate of the organic reagent that would correspond to the observed current increase. This column was calculated assuming one electron was transferred per molecule of substrate oxidized, except for formate, for which a two-electron oxidation was shown (vide infra). The final column contains the ratio of column 4 to column 2. The numbers shown in bold type were obtained using an electrode (TiO_2-1) that was operated at a constant current of 15 mA for the degradation experiments. The current increase experiments were performed at the potential observed during the degradation experiments (3.1 V vs NHE). The data shown in plain type were taken with a different electrode (TiO_2-2) that was operated at a constant potential of 2.9 V vs NHE for both the degradation and current increase experiments. The steady-state currents observed during the degradation experiments using this latter electrode ranged from 9 to 10 mA.

Previous research indicates that the one-electron oxidation

product of formate is unstable and immediately injects another electron into the electrode (a process called "current doubling").[28, 29] Since formate was shown to undergo a two-electron oxidation in our experiments as well, the current increase data were analyzed assuming that two electrons were transferred for each molecule of formate that was consumed from the solution.

direct: $$HCO_2H \rightarrow CO_2 + 2H^+ + 2e^- \quad (4)$$

$^\bullet$OH: $$HCO_2H + {}^\bullet OH \rightarrow {}^\bullet CO_2H + H_2O \quad (5)$$

$$^\bullet CO_2H + {}^\bullet OH \rightarrow CO_2 + H_2O$$

A comprehensive study of the reaction intermediates present in the solution was not performed for the other substrates, and so it is not known how many electrons are transferred per molecule of those substrates. The values given in Table 2 therefore assume only one electron transferred per substrate molecule (except for formate as noted above). If the direct oxidation reactions involve transfer of more than one electron to a given molecule of substrate, then the values for the percentage of direct oxidation quoted in Table 2 will be larger than the actual values (by a factor equal to the number of electrons transferred). These values can, therefore, only serve as upper limits on the actual branching ratio for all substrates except for formate, and they indicate the maximum possible percentage of reaction occurring through a direct oxidation pathway.

The data in Table 2 indicate that formate is consumed primarily through an $^\bullet$OH mechanism under the conditions of our experiments. 4-Chlorophenol and 4-chlorocatechol showed similar degradation rates to each other, as determined by the time dependence of the decrease in substrate concentration. However, 4-chlorocatechol, which is known to adsorb strongly to the surface of TiO_2,[30] causes a larger current increase per unit substrate concentration than does 4-chlorophenol, which does not adsorb to TiO_2.[31−33] These results suggest that a higher percentage of degradation occurs through the direct oxidation process for 4-chlorocatechol degradation than for 4-chlorophenol. The dependence of the results on the specific electrode and/or operating conditions can be seen by comparing the two results shown for acetate (see also Experimental Section). The first electrode indicated that as much as 65% of the degradation may have occurred via direct oxidation, whereas the second electrode showed only 15%. Within the series of experiments for the chlorinated acetates operated under the same conditions, the trend of the current increases agrees with the expected trend in oxidation potentials shown in eq 2. Acetate causes the largest current increase (i.e., is the easiest to oxidize), followed by dichloroacetate and trichloroacetate.

Reaction Kinetics in the Flate Plate Cell. The rates of degradation of sodium azide, *tert*-butyl methyl ether, dichlorophenoxyacetic acid, diisopropylmethylphosphonate, *p*-cresol, formate, and 2-hydroxyethyl sulfide were measured in the flate plate cell operating in the batch mode at $i = 20$ mA cm^{-2} in a background CO_2/HCO_3^- buffer/electrolyte system. The degradation rates of azide, diisopropylmethylphosphonate, and *p*-cresol were found to be strictly first-order for more than 3 half-lives. Furthermore, the measured pseudo-first-order rate constants (i.e., the slopes of the $\ln(C/C_0)$ vs time plots) were in direct proportion to the known second-order reaction rate constants for the corresponding homogeneous aqueous-phase reactions with HO$^\bullet$ (Table 3). On the other hand, the observed first-order plots for azide and formate oxidation showed nonlinear behavior after an initial period of strict first-order behavior. These observations may be related to the fact that they are both small anions and that they were present in relatively large concentrations. Under these conditions, a large concentration of the target substrates may have been present in the electrical double layer and on the surface of the anode. However, the initial slopes of the first-order region will be used for comparative purposes. If we know the value of at least one second-order rate constant, we can determine the other rate constants by the comparative rate method. The results of this calculation are presented in the last column of Table 3. In this case, the rate constant of *p*-cresol with hydroxyl radical is set equal to the literature value $k_{OH} = 1.2 \times 10^9$ M^{-1} s^{-1},[37] and the rate constants are calculated in proportion to the corresponding values of the pseudo-first-order rate constant. The values of k_{OH} for azide and formate are also available from the literature and are compared to the values compiled by Buxton et al.[37] The inferred constant for azide is in excellent agreement with the literature value, but the value for formate is too large by a factor of 2. This discrepancy may be due to the fact that the apparent first-order behavior for formate broke down after 5 min. The computed value for 2-hydroxylethyl sulfide is almost identical to the literature value for diethyl sulfide, and the computed value for diisopropylmethylphosphonate, which has two isopropyl groups, is slightly less twice the value for 2-propanol, and the value for 2,4-dichlorophenoxyacetate is practically equal to the literature value for 4-chlorophenol. The computed value for the rate constant of OH radical with MTBE as determined by the comparative rate method agrees well with the literature value (Table 3). Overall, the correspondence between the rate constants computed from our kinetic data and values in the literature is quite good.

TABLE 3: Comparison of Measured Second-Order Rate Constant for Reactions of Hydroxyl Radical with Substrates at 25 °C and pH 7 in a CO_2/HCO_3^- Buffered System to Literature Values

		measd	
substrate	k_{obs} (s^{-1})	k_{OH} (M^{-1} s^{-1})	lit.
azide, N_3^-	2.01×10^{-3}	1.2×10^{10}	1.2×10^{10}
tert-butyl methyl ether	4.35×10^{-4}	2.5×10^9	1.6×10^9
p-cresol	2.07×10^{-3}	reference	1.2×10^{10}
2,4-D[d]	1.42×10^{-3}	7.9×10^9	7.9×10^9 [a]
DIPMP	5.41×10^{-4}	3.1×10^9	2.3×10^9 [b]
formate, HCO_2^-	1.08×10^{-3}	6.3×10^9	3.2×10^9
$(HOCH_2CH_2)_2S$	2.75×10^{-3}	1.5×10^{10}	1.4×10^{10} [c]

[a] Phenyl acetate. [b] 2-Propanol. [c] $(CH_3CH_2)_2S$. [d] 2,4-Dichlorophenoxyacetate.

Discussion

The large increase in current per unit concentration of acetate observed with electrode TiO_2-1 was surprising given that the trend in degradation rates for the chlorinated acetates (taken with the same electrode and under the same operating conditions) agreed well with the trend expected for an $^\bullet$OH abstraction mechanism. However, as in the case of formate, the direct oxidation of acetate may involve transfer of multiple electrons before intermediates are released from the surface. In the extreme case of complete oxidation for the direct pathway involving transfer of six electrons, only 11% of the loss of acetate would result from direct transfer.

An analysis of the products formed from $^\bullet$OH and photo-Kolbe oxidations of acetate in homogeneous solution has been performed by Schuchmann et al.[34,35] Proposed mechanisms are shown below.

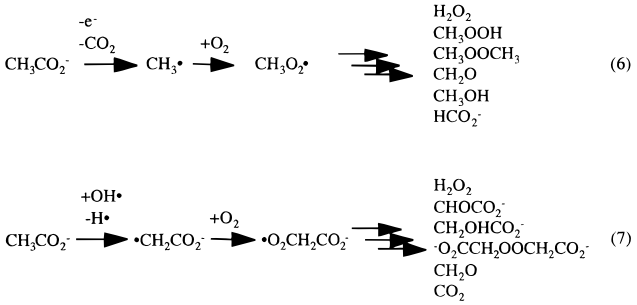

These mechanisms predict differences in the product distribution for the various kinetic pathways under consideration. For example, direct one-electron oxidation of acetate is expected to release one molecule of CO_2 and is also expected to produce a methyl radical that then reacts further with O_2 to produce a variety of intermediates. In contrast, the reaction of acetate with $^{\bullet}OH$ also produces a carbon-centered radical which reacts with O_2, but which produces a different set of intermediates. Furthermore, CO_2 is not an initial product at all in the $^{\bullet}OH$ pathway.

An analysis of the CO_2 production rate in our system during acetate degradation was therefore performed in order to assess the number of electrons transferred per acetate molecule degraded in the direct oxidation mechanism. If a stoichiometric amount of CO_2 were observed, as in the case of formate degradation, then no intermediates are formed, and the direct mechanism must have involved the complete six electron oxidation. However, only one molecule of CO_2 was produced per molecule of acetate degraded. This is consistent with a variety of kinetic pathways and does not allow assignment of the number of molecules transferred per acetate oxidized.

In related work, we performed an extensive analysis of the products formed during acetate oxidation on illuminated ZnO particles.[36] The concentrations of the observed products (i.e., HCO_2^-, $CHOCO_2^-$, CH_3OOH, CH_3COOOH, HCOOH, H_2O_2, and CO_2) were not in accord with expectations from either isolated kinetic pathway observed by von Sonntag and coworkers. In order to explain our results, a surface-mediated oxidation mechanism can be proposed.[36] The direct oxidation pathway (i.e., electron transfer) pathway may proceed as follows:

$$CH_3COO^- + h^+ \rightarrow {}^{\bullet}CH_3 + CO_2 \quad (8)$$

$$CH_3^{\bullet} + O_2 \rightarrow CH_3O_2^{\bullet} \quad (9)$$

$$2CH_3O_2^{\bullet} \rightarrow CH_3OOH + HCO_2H \quad (10)$$

$$CH_3COO^- + H_2O_2 \rightarrow CH_3COOOH + OH^- \quad (11)$$

while the indirect oxidation pathway (hydroxyl radical abstraction) proceeds with the formation of a glyoxalate intermediate:

$$>OH^{\bullet} + CH_3XOO^- \rightarrow >OH_2 + \dot{C}H_2COO^- \quad (12)$$

$${}^{\bullet}CH_2COO^- + O_2 \rightarrow O_2{}^{\bullet}CH_2CO_2^- \quad (13)$$

$$O_2\dot{C}H_2CO_2^- + H_2O \rightarrow HO^{\bullet}{}_2 + HC(OH)_2CO^-{}_2 \quad (14)$$

The intermediate, glyoxalate, is then oxidized via a direct electron transfer pathway to yield the remaining products:

$$HC(OH)_2CO_2^- + h^+ \rightarrow HC(OH)_2CO_2 \quad (15)$$

$$HC(OH)_2CO_2^{\bullet} \rightarrow HC(OH)_2^{\bullet} + CO_2 \quad (16)$$

$$HC(OH)_2^{\bullet} + h^+ \rightarrow HCO_2^- + 2H^+ \quad (17)$$

$$2HO_2^{\bullet} \rightarrow H_2O_2 + O_2 \quad (18)$$

$$HCOCO_2^- + H_2O_2 \rightarrow HCO_2^- + CO_2 + H_2O \quad (19)$$

Our results indicate that both direct hole transfer and $^{\bullet}OH$ abstraction are occurring simultaneously, with direct oxidation accounting for between 11 and 65% of the acetate degraded with electrode TiO_2-1 and only 2−15% of the acetate degraded with electrode TiO_2-2. Due to the similarity of the intermediates produced in the two homogeneous pathways, as well as the complicating factors involved in the potential participation of surface reaction processes, further quantification of the kinetic pathways in our system would be difficult through analysis of the time dependence of concentrations of the intermediates. Thus, for molecules more complex than formate, only an upper limit on the percentage of oxidation that occurs through the direct oxidation pathway can be established.

The hydroxyl radical produced on the surface of the electrodes is nominally bound in the form of a surface titanol functionality, >TiOH. Hydroxyl radical that is not consumed by reactions with substrates within the electrical double layer may self-react to form hydrogen peroxide. In the flate cell reactor configuration, we were operating in the reaction-limited regime, in which the small steady-state concentration of surface-bound hydroxyl radical controls the reaction rate with an observed first-order dependence on the substrate. The steady-state concentration of $>TiOH^{\bullet}$ can be estimated assuming that all of the current passed through the anode produces OH, and the actual concentration would be limited by the recombination reaction leading to H_2O_2 on the surface. The steady-state surface bound hydroxyl radical concentration can be estimated as follows:

$$[H_2O_2]_{ss} = \left(\frac{9 f_{OH} D_{OH} i}{32 k_h{}^2 F_0}\right)^{1/3} \quad (20)$$

where i is the current (1.0 mA cm^{-2}), f_{OH} is the idealized current efficiency for $^{\bullet}OH$ radical production (1.0 mol F_0^{-1}), D_{OH} is the diffusion coefficient for hydroxyl radical (4×10^5 cm^2 s^{-1}), $F_0 = 96\,485$ C mol^{-1}, and k_r is the rate constant for the $^{\bullet}OH$ radical self-reaction to form hydrogen peroxide (5.5×10^9 M^{-1} s^{-1}). Using the above values, the steady-state concentration of hydroxyl radical on the surface is estimated to be 1.6×10^{-13} mol cm^{-2} for a current of 1.0 mA cm^{-2}. This number can be compared to the typical site density of >TiOH groups on colloidal TiO_2 (i.e., 5 sites nm^{-2}), which is about 1×10^{-8} mol cm^{-2}. Thus, a number of potential binding sites remain for sorption by the substrates that allow for the possibility of simultaneous direct electron transfer reactions.

Conclusions

The observed trend in acetate degradation rates as well as the increase in current per unit substrate concentration increase indicates the production of $^{\bullet}OH$ at degenerately doped polycrystalline TiO_2 electrodes under strong anodic bias. The electrochemical data allow for the quantification of the extent of direct and $^{\bullet}OH$ radical pathways for the degradation of a variety of compounds under our experimental conditions. In addition, current increase experiments suggest that surface

adsorption plays an important role in determining the oxidation mechanisms in TiO_2 catalysis. Experiments with TiO_2 electrodes operated in the light at less positive potentials could also be used to determine these quantities for TiO_2 photocatalysis. The results may differ due to different surface interactions at the high potentials used in the electrocatalysis experiments. However, this approach should provide useful information in designing optimal waste treatment systems.

Acknowledgment. We are grateful to DARPA and ONR {NAV 5 HFMN N0001492J1901} for financial support. J. Kesselman acknowledges the NSF for a predoctoral fellowship.

References and Notes

(1) Ollis, D. F. In *Homogeneous and Heterogeneous Photocatalysis*; Pelizzetti, E., Serpone,N., Eds.; D. Reidel Publishing: Dordrecht, 1986; pp 651−656.

(2) Hoffmann, M. R.; Martin, S. T.; Choi, W.; Bahnemann, D. W. *Chem. Rev.* **1995**, *95*, 69−96.

(3) Finklea, H. O. In *Semiconductor Electrodes*; Finklea, H. O. Ed.; Elsevier: New York, 1988; pp 43−146.

(4) Nozik, A. J. *Annu. Rev. Phys. Chem.* **1978**, *29*, 189−222.

(5) Pruden, A. L.; Ollis, D. F. *Environ. Sci. Technol.* **1983**, *17*, 628−631.

(6) Hidaka, H.; Nohara, K.; Zhao, J.; Serpone, N.; Pelizzetti, E. *J. Photochem. Photobiol. A: Chem.* **1992**, *64*, 247−254.

(7) Hidaka, H.; Zhao, J.; Kitamura, K.; Nohara, K.; Serpone, N.; Pelizzetti, E. *J. Photochem. Photobiol. A: Chem.* **1991**, *64*, 103−113.

(8) Terzian, R.; Serpone, N.; Minero, C.; Pelizzetti, E.; Hidaka, H. *J. Photochem. Photobiol. A: Chem.* **1990**, *55*, 243−249.

(9) Choi, W.; Termin, A.; Hoffmann, M. R. *J. Phys. Chem.* **1994**, *98*, 13669−13679.

(10) Kormann, C.; Bahnemann, D. W.; Hoffmann, M. R. *Environ. Sci. Technol.* **1991**, *25*, 494−500.

(11) Al-Ekabi, H.; Safarzadeh-Amiri, A.; Sifton, W.; Story, J. *Int. J. Environ. Pollut.* **1991**, *1*, 125−136.

(12) Weres, O.; Hoffmann, M. R. Electrode, Electrode Manufacturing Process and Electrochemical Cell. U.S. Patent 5,419,824, May 30, 1995.

(13) Weres, O.; Hoffmann, M. R. Electrochemical Method and Device for Generating Hydroxyl Free Radicals and Oxidizing Chemical Substances Dissolved in Water. U.S. Patent 5,364,508, Nov. 15, 1994.

(14) Weres, O.; Hoffmann, M. R. Electrochemical Device for Generating Hydroxyl Free Radicals and Oxidizing Chemical Substances Dissolved in Water. U.S. Patent 5,439,577, Aug. 8, 1995.

(15) Vinodgopal, K.; Stafford, U.; Gray, K. A.; Kamat, P. V. *J. Phys. Chem.* **1994**, *98*, 6797−6803.

(16) Vinodgopal, K.; Hotchandani, S.; Kamat, P. V. *J. Phys. Chem.* **1993**, *97*, 9040−9044.

(17) Kläning, U. K.; Sehested, K.; Holcman, J. *J. Phys. Chem.* **1985**, *89*, 760−763.

(18) Kesselman, J. M.; Shreve, G. A.; Hoffmann, M. R.; Lewis, N. S. *J. Phys. Chem.* **1994**, *98*, 13385−13395.

(19) Nishimoto, S.-i.; Ohtani, B.; Kagiya, T. *J. Chem. Soc., Faraday Trans. 1* **1985**, *81*, 2467−2474.

(20) Prairie, M. R.; Evans, L. R.; Stange, B. M.; Martinez, S. L. *Environ. Sci. Technol.* **1993**, *27*, 1776−1782.

(21) Micic, O. I.; Zhang, Y.; Cromack, K. R.; Trifunac, A. D.; Thurnauer, M. C. *J. Phys. Chem.* **1993**, *97*, 7277−7283.

(22) Draper, R. B.; Fox, M. A. *Langmuir* **1990**, *6*, 1396−1402.

(23) Stafford, U.; Gray, K. A.; Kamat, P. V. *J. Phys. Chem.* **1994**, *98*, 6343−6351.

(24) Goldstein, S.; Czapski, G.; Rabani, J. *J. Phys. Chem.* **1994**, *98*, 6586−6591.

(25) Mao, Y.; Schöneich, C.; Asmus, K.-D. *J. Phys. Chem.* **1991**, *95*, 10080−10089.

(26) Brezova, V.; Stasko, A. L. Lapcik, J. *J. Photochem. Photobiol. A: Chem.* **1991**, *59*, 115−121.

(27) Samuni, A.; Carmichael, A. J.; Russo, A.; Mitchell, J. B.; Riesz, P. *Proc. Natl. Acad. Sci. U.S.A.* **1986**, *83*, 7593−7597.

(28) Kerchove, F. V.; Vandermolen, J.; Gomes, W. P.; Cardon, F. *Ber. Bunsen-Ges. Phys Chem.* **1979**, *83*, 230−236.

(29) Dutoit, E. C.; Cardon, F.; Gomes, W. P. *Ber. Bunsen-Ges. Phys. Chem.* **1976**, *80*, 1285−1288.

(30) Martin, S. T.; Kesselman, J. M.; Park, D. S.; Lewis, N. S.; Hoffmann, M. R. *Environ. Sci. Technol.* **1996**, *30*, 2535−2542.

(31) Tunesi, S.; Anderson, M. *J. Phys. Chem.* **1991**, *95*, 3399−3405.

(32) Mills, A.; Morris, S. *J. Photochem. Photobiol. A: Chem.* **1993**, *71*, 75−83.

(33) Cunningham, J.; Sedlák, P. *J. Photochem. Photobiol. A: Chem.* **1994**, *77*, 255−263.

(34) Schuchmann, H.-P.; Sonntag, C. v. *Z. Naturforsch.* **1984**, *39b*, 217−221.

(35) Schuchmann, M. N.; Zegota, H.; Sonntag, C. v. *Z. Naturforsch.* **1985**, *40B*, 215−221.

(36) Carraway, E. R.; Hoffman, A. J.; Hoffmann, M. R. *Environ. Sci. Technol.* **1994**, *28*, 786−793.

(37) Buxton, G. V.; Greenstock, C. L.; Helman, W. P.; Ross, A. B. *J. Phys. Chem. Ref. Data* **1988**, *17*, 513−886.